Metabolic profile of synthetic cannabinoids 5F-PB-22, PB-22, XLR-11 and UR-144 by *Cunninghamella elegans*

Shimpei Watanabe[a], Unnikrishnan Kuzhiumparambil[a,b], My Ann Nguyen[a], Jane Cameron[c] and Shanlin Fu[a*]

[a] *Centre for Forensic Science, School of Mathematical and Physical Sciences, University of Technology Sydney (UTS), PO Box 123, Broadway, NSW 2007, Australia*

[b] *Plant Functional Biology and Climate Change Cluster, University of Technology Sydney (UTS), PO Box 123, Broadway, NSW 2007, Australia*

[c] *Cell Biology Facility, University of Technology Sydney (UTS), PO Box 123, Broadway, NSW 2007, Australia*

* Corresponding author: Shanlin Fu

Mailing address: Centre for Forensic Science

School of Mathematical and Physical Sciences

University of Technology Sydney (UTS)

PO Box 123, Broadway NSW 2007 Australia

E-mail: Shanlin.fu@uts.edu.au

Phone: +61 2 9514 8207

Fax: +61 2 9514 2260

Abstract

The knowledge of metabolic profile of synthetic cannabinoids is important for the detection of the drugs in urinalysis due to the typical absence or low abundance of parent cannabinoids in human urine. The fungus *Cunninghamella elegans* has been reported to be a useful tool for metabolism study and thus applicability to synthetic cannabinoids metabolism was examined. In this study, 8-quinolinyl 1-(5-fluoropentyl)-1H-indole-3-carboxylate (5F-PB-22), 8-quinolinyl 1-pentyl-1H-indole-3-carboxylate (PB-22), [1-(5-fluoropentyl)-1H-indol-3-yl](2,2,3,3-tetramethylcyclopropyl)methanone (XLR-11) and (1-pentyl-1H-indol-3-yl)(2,2,3,3-tetramethylcyclopropyl)methanone (UR-144) were incubated with *Cunninghamella elegans* and the metabolites were identified using liquid chromatography-quadrupole time-of-flight mass spectrometry. The obtained metabolites were compared with reported human metabolites to assess the suitability of the fungus to extrapolate human metabolism. 5F-PB-22 underwent, dihydroxylation, dihydrodiol formation, oxidative defluorination, oxidative defluorination to carboxylic acid, ester hydrolysis and glucosidation, alone and/or in combination. The metabolites of PB-22 were generated by hydroxylation, dihydroxylation, trihydroxylation, dihydrodiol formation, ketone formation, carboxylation, ester hydrolysis and glucosidation, alone and/or in combination. XLR-11 was transformed through hydroxylation, dihydroxylation, aldehyde formation, carboxylation, oxidative defluorination, oxidative defluorination to carboxylic acid and glucosidation, alone and/or in combination. UR-144 was metabolised by hydroxylation, dihydroxylation, trihydroxylation, aldehyde formation, ketone formation, carboxylation, *N*-dealkylation and combinations. These findings were consistent with previously reported human metabolism except for the small extent of ester hydrolysis observed and absence of glucuronidation. Despite the limitations, *Cunninghamella elegans* demonstrated the capacity to produce a wide variety of metabolites including some major human metabolites of XLR-11 and UR-144 at high abundance, showing the potential for metabolism of newly emerging synthetic cannabinoids.

Keywords: Synthetic cannabinoids, Metabolism, *Cunninghamella elegans*, 5F-PB-22, XLR-11

Abbreviations

CB_1	Cannabinoid type 1
CB_2	Cannabinoid type 2
C. elegans	*Cunninghamella elegans*
ESI	Electrospray ionization source
5F-PB-22	8-quinolinyl 1-(5-fluoropentyl)-1H-indole-3-carboxylate
5F-PI-COOH	5-fluoropentylindole-3-carboxylic acid
HLM	Human liver microsomes
LC-QqQ	Liquid chromatography-triple quadrupole
LC-QTOF-MS	Liquid chromatography-quadrupole time-of-flight mass spectrometry
MS	Mass spectrometry
NMR	Nuclear magnetic resonance
PB-22	8-quinolinyl 1-pentyl-1H-indole-3-carboxylate
PI-COOH	Pentylindole-3-carboxylic acid
TMCP	Tetramethylcyclopropyl
UR-144	(1-pentyl-1H-indol-3-yl)(2,2,3,3-tetramethylcyclopropyl)methanone
XLR-11	[1-(5-fluoropentyl)-1H-indol-3-yl](2,2,3,3-tetramethylcyclopropyl)methanone

Introduction

New psychoactive substances have been increasingly appearing on the drug market. In particular, synthetic cannabinoids are the major class of drugs and over 160 compounds have been detected since 2008 with 24 of them appearing for the first time in 2015 [1]. Synthetic cannabinoids are cannabinoid type 1 (CB_1) and type 2 (CB_2) receptor agonists like Δ^9-tetrahydrocannabinol, the active ingredient of cannabis, producing psychoactive effects but can be significantly more potent since cannabinoids and metabolites often have higher affinity and full agonist activity for both CB_1 and CB_2 receptor [2, 3]. As such, adverse health effects including seizures, psychosis, hallucinations, cardiotoxic effects, coma and deaths have been associated with the use of synthetic cannabinoids and it has become a serious public health concern [4].

Due to the emergence of many synthetic cannabinoids within a short period, understanding of their pharmacology including metabolism is still limited. Knowledge of metabolites is important for forensic and clinical cases to prove the consumption of particular cannabinoids in urinalysis because synthetic cannabinoids are generally extensively metabolised and are usually not found without modification or found in low abundance in urine, requiring abundant and specific metabolites to be targeted instead [5-14].

Different approaches have been taken for metabolite identification studies. While providing the most reliable data [15], self-administration of drugs is difficult due to possible side effects and ethical concerns and therefore other approaches are commonly taken such as *in vitro* human hepatocytes [7-9, 16-20] and human liver microsomes (HLM) [6, 14, 21-26], and *in vivo* animals [5, 25-27]. The combination of controlled experiments such as human hepatocytes and authentic human urine analysis particularly appears to be valuable [28, 29]. However, cost, maintenance, species differences and/or ethics can be an issue with these models [30]. Furthermore, quantity of metabolites obtained is usually not sufficient for isolation [30], limiting the analysis to the use of mass spectrometry. However, unambiguous structural elucidation may not be possible without techniques such as nuclear magnetic resonance (NMR) spectroscopy [29].

While less common, the potential of microbial models for metabolic studies have been investigated over the past few decades [30]. *Cunninghamella elegans* (*C. elegans*) is a fungus species known to metabolise many xenobiotics regio- and stereo-selectively, similar to mammalian metabolism [30]. The fungus has enzymatic activity for both phase I and II enzymes [31] and possesses cytochrome P450 enzymes known as CYP509A1, which are close to CYP51 family [32]. While little is known about the activity of CYP509A1, the fungus is capable of various reactions, such as hydroxylation, carboxylation, dihydrodiol formation, oxidative defluorination, *N*-dealkylation, glucosidation and sulfation [30, 33], including those catalysed by human CYP1A2, CYP2C9, CYP2C19 and CYP2D6 [2, 33-37]. CYP3A4 is reported to be the major enzyme involved in the metabolism of [1-(5-fluoropentyl)-1H-indol-3-yl](2,2,3,3-tetramethylcyclopropyl)methanone (XLR-11) and (1-pentyl-1H-indol-3-yl)(2,2,3,3-tetramethylcyclopropyl)methanone (UR-144), two of the drugs investigated in this study, while CYP1A2 has a minor influence. There is no literature on specific enzymes responsible for the metabolism of 8-quinolinyl 1-(5-fluoropentyl)-1H-indole-3-carboxylate (5F-PB-22) and 8-quinolinyl 1-pentyl-1H-indole-3-carboxylate (PB-22), the other two drugs investigated. Some of the advantages of *C. elegans* include low cost, no

ethical concern involved, simple and cheap maintenance of stock fungal cultures that can be subcultured, high reproducibility, diverse metabolic profile and larger amounts of metabolite produced, which might result in more fragment ions in mass spectrometric analysis, facilitating structural elucidation [30, 38]. More importantly, production of large amounts of metabolites have allowed for the structural characterisation of metabolites by NMR spectroscopy [39, 40]. Therefore, *C. elegans* may prove useful for synthetic cannabinoids metabolism study, especially where reference standards for metabolites of new compounds are not available.

The purpose of the study was to identify the metabolites of 5F-PB-22, PB-22, XLR-11 and UR-144 by *C. elegans* and to compare the fungal metabolites with human *in vivo* and *in vitro* metabolites reported in literature to examine whether *C. elegans* might have the possibility to be used as a complementary model for metabolism studies of synthetic cannabinoids with production of appropriate human metabolites. We have previously investigated the metabolism of synthetic cannabinoids JWH-018, JWH-073 and AM2201 by *C. elegans* and their metabolic profiles were in good agreement with human metabolism, producing majority of the phase I human metabolites [33, 41]. The four synthetic cannabinoids were chosen because they have different structural classes from the cannabinoids in our previous study and human *in vivo* and/or *in vitro* metabolism data are available. Metabolites were analysed by liquid chromatography-quadrupole time-of-flight mass spectrometry (LC-QTOF-MS) with the aid of liquid chromatography-triple quadrupole (LC-QqQ) mass spectrometry. LC-QTOF-MS was mainly employed because it provides high-resolution mass spectrometric data, increasing the confidence of characterisation of metabolites by distinguishing isobaric compounds.

Materials and Methods

Chemicals and reagents

5F-PB-22 and PB-22 were obtained from PM separations (Capalaba, QLD, Australia) and XLR-11 and UR-144 were from the National Measurement Institute (North Ryde, NSW, Australia). Reagent grade dichloromethane, LC grade acetonitrile, acetone and sodium chloride were obtained from Chemsupply (Gilman, SA, Australia). LC-MS grade formic acid was obtained from Sigma–Aldrich (St. Louis, MO, USA). Glycerol and potassium dihydrogen orthophosphate were from Ajax Chemicals (Auburn, NSW, Australia). Potato dextrose agar, glucose, peptone, and yeast extract were purchased from Oxoid Australia (Adelaide, SA, Australia).

Biotransformation by fungus and sample preparation

C. elegans ATCC 10028b (Cryosite Ltd., South Granville, NSW, Australia) was cultured on potato dextrose agar plates at 27 °C for 5 days ensuring the whole plates were covered with mycelia. The mycelia were then transferred to sterile physiological saline solution (1 plate of mycelia per 5 mL) and homogenized for 5 min. Approximately 1.5 mL aliquots of the homogenate were inoculated into 100 mL growth media, prepared according to the methods in [42], in 250 mL Erlenmeyer flasks. The cultures were incubated for 48 h at 26 °C and 180

rpm on an Infors HT Multitron rotary shaker (In vitro Technologies, Noble Park North, VIC, Australia). After 48 h, 0.5 mL of 5F-PB-22, PB-22, XLR-11 or UR-144 in acetone (2 mg/mL) was added to the culture and incubated for further 72 h. Two control samples were also incubated and consisted of 1) media and fungus without drugs to determine compounds unrelated to the drugs and 2) media and drug without fungus.to determine degradation of the drugs.

After 72 h, fungus was removed by filtration using Buchner funnel and the remaining solution was extracted with dichloromethane (3 × 50 mL). The extracts were combined and evaporated to dryness using a Buchi rotary evaporator (In vitro Technologies, Noble Park North, VIC, Australia) followed by a vacuum pump. Each samples was reconstituted in 2 mL acetonitrile and was further diluted in acetonitrile by 10-fold before injecting to LC-MS.

LC-QTOF analysis

Chromatographic separation of samples was performed using an Agilent 1290 LC system with an Agilent Zorbax Eclipse XDBC18 analytical column (150 mm × 4.6 mm, 5 µm). Mobile phases were 0.1% formic acid in water (A) and 0.1% formic acid in acetonitrile (B) at a flow rate of 0.4 mL/min. Due to the difference in polarity of the cannabinoids, two mobile phase gradients were used. For 5F-PB-22 and PB-22, 30% B was held until 1 min, ramped to 50% B at 3 min, 90% B at 20 min and held until 24 min, then ramped down to 30% B at 25 min and held for re-equilibration until 30 min. For XLR-11 and UR-144, 30% B was held until 1 min, ramped to 60% B at 3 min, to 90% B at 20 min and held until 24 min, and ramped down to 30% B at 25 min for re-equilibration until 30 min. Injection volume was 4 µL (MS mode) and 10 µL (targeted MS/MS mode).

Mass spectrometric data was acquired on an Agilent 6510 Accurate Mass Q-TOF Mass Spectrometer, equipped with an electrospray ionization source (ESI) source operated in positive ion mode. The following parameters were used: scanning mass range, *m/z* 100–1000 (MS), *m/z* 100–950 (MS/MS); capillary voltage, 3500 V; nebulizer pressure, 30 psig; gas flow, 5 L/min; gas temperature, 325 °C; fragmentor voltage, 160 V (XLR-11, UR-144), 80 V (5F-PB-22, PB-22); collision energy, 10, 20 and 40 eV; skimmer voltage, 65 V. Mass calibration was performed over the m/z 50–3200 range with the mixture provided by the manufacturer. Automated real-time calibration during runs was in place using the following reference masses: m/z 121.0509 and m/z 922.0098.

Chromatographic and mass spectrometric data was analysed using Agilent MassHunter Workstation Software Qualitative Analysis (version B.06.00) for MS scan both manually looking at peaks present in fungus samples but absent in controls and with a PCDL library created by Agilent MassHunter PCDL Manager (version B.04.00) with known metabolites of the drugs to search for the potential metabolites. MS/MS scans were performed on the precursor ions which were suspected to be metabolites. Search parameters were as follows: mass tolerance, 20 ppm; maximum number of matches, 8; absolute peak area ≥ 5000. The criteria for metabolites were as follows: mass error of the protonated ion ≤ 5.1 ppm; consistent fragmentation pattern with proposed structure; reasonable retention time relative to other biotransformations; absence of the specific peak in controls.

LC-QqQ analysis

An Agilent 6490 Triple Quadrupole mass spectrometer with ESI source (positive ion mode) coupled with an Agilent 1290 LC system was used for product ion scans for a few PB-22 metabolites (*m/z* 405 and 409) where some fragment ions for the potential metabolites were absent in QTOF analysis. Data derived from QqQ analysis is indicated in **Supplementary Table II**. All the chromatographic conditions and column used were the same as for QTOF analysis except for the injection volume of 2 µL. The following mass spectrometric conditions were used: scanning mass range, *m/z* 85–500; fragmentor voltage, 380 V; collision energy, 10, 20, 30 and 40 eV; gas temperature, 200 °C; gas flow, 14 L/min; capillary voltage, 3000 V.

Results

5F-PB-22 metabolites found after fungus incubation are listed in **Supplementary Table I** including proposed biotransformation, retention time, elemental composition, exact mass, accurate mass, mass error, and diagnostic product ions. Similarly, PB-22, XLR-11, and UR-144 metabolites are listed in **Supplementary Tables II, III, and IV**, respectively. **Fig. 1** shows MS/MS spectra as well as their structures with suggested fragmentation patterns of 5F-PB-22, PB-22, XLR-11 and UR-144 and their major metabolites.

5F-PB-22

Sixteen metabolites (labelled as F1 – F16 in the order of retention time) were detected after incubation with *C. elegans*. They eluted between 6.4 min and 12.6 min before the parent drug at 17.6 min (**Fig. 2a**). The metabolites were generated by dihydrodiol formation (F10) followed by hydroxylation (F3), dihydroxylation (F7-F9), hydroxylation (F14-F16), oxidative defluorination to carboxylic acid (F13) followed by hydroxylation (F5, F6, F11), oxidative defluorination with dihydrodiol (F1), ester hydrolysis resulting in 5-fluoropentylindole-3-carboxylic acid (5F-PI-COOH, F12) followed by glucosidation (F2) or hydroxylation (F4). The mass errors of the metabolites based on the proposed biotransformations were all within 1.39 ppm. The top three abundant metabolites based on peak area were dihydrodiol (F10), hydroxylation (F15) and oxidative defluorination to carboxylic acid (F13). Proposed metabolic pathway of 5F-PB-22 is shown in **Fig. 3**. Comparison of the fungal metabolites in this study with human hepatocytes and HLM metabolites in the literature is shown in **Table I**.

PB-22

A total of 30 metabolites (P1-P30) were found to elute between 6.2 min and 15.1 min all before the parent drug at 21.7 min (**Fig. 2b**). The following biotransformation was observed: carboxylation (P24) followed by hydroxylation (P12), dihydrodiol formation (P27) followed by hydroxylation (P3, P7) or ketone formation (P8, P14), dihydroxylation (P13, P15, P16, P19), hydroxylation (P26, P28), ketone formation (P29, P30) followed by hydroxylation (P17,

P20-P23, P25) and glucosidation (P1) or dihydroxylation (P4, P5, P9, P18), trihydroxylation (P2), ester hydrolysis leading to pentylindole-3-carboxylic acid (PI-COOH) followed by hydroxylation (P6, P11) or glucosidation (P10). The mass errors of all the metabolites were 2.51 ppm or less. Three major fungal metabolites were dihydroxylation (P13), dihydrodiol formation with ketone formation (P8) and dihydroxylation (P16). Proposed metabolic pathway of PB-22 is shown in **Fig. 4**. Comparison of the fungal metabolites in this study with human hepatocytes and HLM metabolites in the literature is shown in **Table II**.

XLR-11

Twenty six metabolites (X1-X26) were observed between 7.6 min and 14.6 min with the parent drug eluting at 20.9 min (**Fig. 2c**). XLR-11 was found to undergo aldehyde formation (X26), carboxylation (X22) followed by glucosidation (X14, X18) or hydroxylation (X10), hydroxylation (X21, X23), dihydroxylation (X3, X6, X9, X11-X13, X19, X20), oxidative defluorination (X25) followed by aldehyde formation (X16) or carboxylation (X8) or hydroxylation (X2, X7), oxidative defluorination to carboxylic acid (X24) followed by aldehyde formation (X15, X17) or carboxylation (X5) or hydroxylation (X1, X4). The mass errors of all the metabolites were within 5.10 ppm. Three most abundant metabolites were hydroxylation (X21), carboxylation (X22) and hydroxylation (X23). Proposed metabolic pathway of XLR-11 is shown in **Fig. 5**. The fungal metabolites in this study are compared with the metabolites in human urine, human hair, human hepatocytes, HLM and HepaRG cells that have been reported in the literature (**Table III**).

UR-144

Twenty five metabolites (U1-U25) were detected, eluting between 6.2 min and 17.4 min before the parent drug at 26.1 min (**Fig. 2d**). The biotransformation included aldehyde formation followed by hydroxylation (U19) or ketone formation (U21), carboxylation followed by hydroxylation (U6, U8, U10, U12, U15), dihydroxylation (U7, U11, U13, U16), hydroxylation (U22-U25), ketone formation followed by carboxylation (U17, U20) or hydroxylation (U14, U18), *N*-dealkylation followed by hydroxylation (U4, U9), trihydroxylation (U1-U3, U5). The mass errors of the proposed metabolites were all within 2.04 ppm. Top three abundant metabolites were dihydroxylation (U7), dihydroxylation (U11) and carboxylation with hydroxylation (U10). Proposed metabolic pathway of XLR-11 is shown in **Fig. 6**. The observed fungal metabolites are compared with the metabolites in human urine and HLM reported in the literature (**Table IV**).

Discussion

Metabolite identification

5F-PB-22

In MS/MS scan, 5F-PB-22 was fragmented to the ions at *m/z* 144 (an unchanged indole moiety) and 232 (an unaltered 5-fluoropentylindole moiety) and they were used as the basis for determining the structures of the metabolites (**Fig. 1)**. All three hydroxy metabolites (*m/z* 393, F14-F16) were found to be hydroxylated at the fluoropentyl side chain indicated by the fragment ions at *m/z* 144 representing an unchanged indole ring and at *m/z* 248 representative of a hydroxylated fluoropentylindole moiety. Two dihydroxy metabolites (*m/z* 409, F7, F8) showed fragment ions at *m/z* 144 and 248 indicating hydroxylation once at the fluoropentyl side chain and another at the quinoline moiety. F9 was another dihydroxy metabolite, hydroxylated twice at the fluoropentylindole moiety as shown by the fragment ion at *m/z* 264. But the lack of fragment ions corresponding to the indole moiety limited further determination as to whether hydroxylation took place at the fluoropentyl side chain, the indole moiety or at both. A metabolite with dihydrodiol formation (*m/z* 411, F10) was characterised by the fragment ions at *m/z* 144 and 232 (**Fig. 1**), suggesting dihydrodiol formation at the quinoline moiety. Further hydroxylation of F10 led to the metabolite (*m/z* 427, F3) with a hydroxy group at the fluoropentylindole moiety as indicated by the fragment ion at *m/z* 248.

Oxidative defluorination to carboxylic acid (*m/z* 389, F13) was suggested by the fragment ions at *m/z* 144 (an unaltered indole ring) and 244 (a carboxylated pentylindole moiety). These fragments themselves only indicate that 5F-PB-22 was defluorinated and that the pentyl side chain has two additional oxygen atoms and two less hydrogen atoms. However, it is probably an *N*-pentanoic acid as it is reported to be a major metabolite of 5F-PB-22 in human hepatocytes studies by Wohlfarth *et al*. [17]. Also, oxidative defluorination to carboxylic acid is a biotransformation previously observed for a synthetic cannabinoid AM2201 by *C. elegans* [33]. Further hydroxylation of F13 resulted in F5, F6 and F11 (*m/z* 405). F5 and F11 were hydroxylated at the quinoline moiety as the fragment ions at *m/z* 144 and 244 were still present. F6 was hydroxylated at the indole moiety, indicated by the fragment ions at *m/z* 160 (a hydroxylated indole ring) and 260 (a hydroxylated and carboxylated pentylindole). Although oxidative defluorination by itself was not observed, a metabolite with oxidative defluorination and dihydrodiol formation was indicated (*m/z* 409, F1). The only fragment ion detected was at *m/z* 230 suggesting a quinoline moiety with dihydrodiol formation and a pentylindole moiety with a hydroxy group. Despite the lack of the *m/z* 144 fragment ion, the position of the hydroxy group can be considered to be at the terminal carbon of the pentyl side chain since oxidative defluorination is a commonly reported pathway to simultaneously defluorinate and hydroxylate fluorinated synthetic cannabinoids [2, 6, 7, 16, 18, 19] and it has been reported for *C. elegans* [33].

Ester hydrolysis led to the 5F-PI-COOH metabolite (*m/z* 250, F12) as indicated by the fragment ions at *m/z* 118 and 232 suggesting an unchanged indole moiety and unmodified 5-fluoropentylindole moiety, respectively. There was another unknown peak with *m/z* 250 in the extracted ion chromatogram, but careful examination of mass spectrum in full scan mode revealed the presence of a coeluting protonated ion at *m/z* 412, which has mass error of 1.39

ppm for a glucoside of F12. Thus, it seems to be a glucoside of 5F-PI-COOH with in-source fragmentation (*m/z* 412, F2). In-source fragmentation of acyl glucuronides is reported for synthetic cannabinoid metabolites including 5F-PB-22 [16, 17] and is likely to occur with glucosides. A metabolite resulting from hydroxylation of F12 was shown by the fragment ions at *m/z* 248 indicating a 5-fluorohydroxypentylindole moiety and 134 corresponding to a hydroxyindole moiety (*m/z* 266, F4).

PB-22

PB-22 was fragmented similarly to 5F-PB-22 and resulted in two product ions at *m/z* 144 and 214 (**Fig. 1**), corresponding to an unchanged indole ring and an unaltered pentylindole moiety. Both hydroxy metabolites (*m/z* 375, P26, P28) underwent hydroxylation at the pentyl side chain as shown by the fragment ions at *m/z* 144 and 230 with the latter indicating a hydroxylated pentylindole moiety. A dihydroxy metabolite (*m/z* 391, P13) showed the fragment ions at *m/z* 144 and 230 (**Fig. 1**), indicating hydroxylation at both the pentyl side chain and the quinoline moiety while the other three dihydroxy metabolites (P15, P16, P19) were hydroxylated twice at the pentyl side chain as suggested by the fragment ions at *m/z* 144 and 246. A trihydroxylated metabolite (*m/z* 407, P2) was indicated to have two hydroxy groups at the pentyl side chain and another at the quinoline moiety (*m/z* 144, 246). A metabolite with dihydrodiol formation at the quinoline moiety (*m/z* 393, P27) was suggested by the ions at *m/z* 144 and 214 representing an unchanged pentylindole moiety. Hydroxylation of P27 at the pentyl side chain resulted in (*m/z* 393, P3, P7) as indicated by the ions at *m/z* 144 and 230. The retention time and fragmentation pattern of P3 and F1 indicated they are identical, suggesting the position of hydroxylation at the terminal carbon. Notably, for P7 the fragment ion at *m/z* 230 was not observed likely because the ion suppression occurred due to the coeluting metabolite P8 (peaks at *m/z* 228 and 229 are seen in the MS/MS, data not shown). However, product ion scan by the LC-QqQ revealed a clear peak at *m/z* 230. Further oxidation of P3 and P7 appeared to form metabolites with a ketone group at the pentyl side chain with dihydrodiol at the quinoline moiety as evidenced by the fragment ions at *m/z* 144 and 228.

Metabolites with a ketone group at the pentyl side chain (*m/z* 373, P29, P30) were characterised by the fragment ions at *m/z* 144 and 228, the latter indicating a pentylindole moiety with a ketone group. Further hydroxylation occurred at the quinoline moiety for P17, P20, P22 and P25 (*m/z* 389) indicated by the fragment ions at *m/z* 144 and 228 and at the pentyl side chain for P21 and P23 suggested by the fragment ions at *m/z* 144 and 244. A glucoside of a hydroxylated metabolite with ketone was detected (*m/z* 551, P1) but it was not a glucoside of any of the phase I metabolites found as the position of the hydroxylation for this metabolite was at the indole moiety (*m/z* 160, 244). Four metabolites with a ketone group at the side chain and dihydroxylation (*m/z* 405, P4, P5, P9, P18) were formed. P4 has a hydroxy group each at the indole ring and the quinoline moiety (*m/z* 160, 244), P5 and P9 at the pentyl side chain and the quinoline moiety (*m/z* 144, 244) and P18 twice at the pentyl side chain (*m/z* 144, 260). For P9 and P18, the fragment ion at *m/z* 144 was absent but was confirmed by the LC-QqQ analysis. P24 (*m/z* 389) showed the fragment ions at *m/z* 144, 244 and based on the retention time and fragmentation pattern it was considered to be identical to

F13 and is proposed to be an *N*-pentanoic acid metabolite. Also, P12 was determined to be identical to F5 and is proposed to be formed by hydroxylating P24 at the quinoline ring.

Similarly to 5F-PB-22, a glucoside of PI-COOH formed from ester hydrolysis (*m/z* 394, P10) was largely fragmented to *m/z* 232 by in-source fragmentation. Several fragment ions including *m/z* 118 and 214 suggested an unchanged pentylindole moiety. PI-COOH with hydroxylation at the pentyl side chain (*m/z* 248, P6, P11) was represented by the fragment ions at *m/z* 130 (an unaltered indole) and 230.

XLR-11

The structure of XLR-11 is similar to 5F-PB-22 with the quinoline moiety replaced by the tetramethylcyclopropyl (TMCP) ring. As such, the fragmentation pattern of XLR-11 was similar; *m/z* 144, 232 and additionally 125 (**Fig. 1**), corresponding to the TMCP moiety were observed. Hydroxylated metabolites (*m/z* 346, X21, X23) were found to have a hydroxy group at the TMCP ring as indicated by the fragment ions at *m/z* 144 and 232 (**Fig. 1**). The absence of the fragment ion at *m/z* 125 also indicated the modification at the TMCP ring. There are three possible positions of hydroxylation: the alpha carbon to the carbonyl group, two methyl groups on the same side of the cyclopropyl ring as the hydrogen atom on the alpha carbon, which is an (*E*)-isomer, and two methyl groups on the other side of the ring from the hydrogen, a (*Z*)-isomer. Wohlfarth *et al*. reported, in their human hepatocytes studies, three hydroxy glucuronides with the two diastereomers eluting closely [16]. Thus, it is possible that the diastereomers might have coeluted under the chromatographic condition employed, resulting in two apparent peaks. Eight dihydroxy metabolites (*m/z* 362, X3, X6, X9, X11-X13, X19, and X20) were detected. X3, X9 and X11 were hydroxylated once each at the fluoropentyl side chain and at the TMCP ring (*m/z* 144, 248) and X6, X12, X13, X19 and X20 twice at the TMCP ring (*m/z* 144, 232). Aldehyde formation at the TMCP ring (*m/z* 344, X26) was characterised by the fragment ions at *m/z* 144 and 232. In fact, aldehydes are highly reactive and might undergo subsequent reaction before being detected. However, intermediate aldehyde metabolite of ebastine is reported to be isolated and characterised along with subsequent carboxylic acid metabolite after incubation with *Cunninghamella blakesleeana*, another species of the genus *Cunninghamella* [43], and therefore aldehyde is tentatively proposed in this study.

Three metabolites (*m/z* 360, X14, X18, X22) were observed with the fragment ions at *m/z* 144 and 232 corresponding to carboxylic acid at the TMCP ring. Similar to hydroxylation of the TMCP ring, there appears to be two possible positions for carboxylation at methyl carbons generating (*E*)- and (*Z*)-isomers. However, this does not explain the presence of three metabolites. Therefore, it is likely that one or two of the three metabolites are phase II metabolites with in-source fragmentation. As the retention time of X22 is relatively late compared to the other two, it is possible that X22 is a carboxy metabolite and X14 and X18 are glucosides of carboxy metabolites. The reason for only one chromatographic peak for the carboxy metabolite may be explained by coelution whereas the phase II metabolites may have sufficient difference in property to be separated by chromatography under the condition employed. Wohlfarth *et al*. also reported the presence of single carboxy metabolite and it was

the peak eluting last among the metabolites with *m/z* 360 and their glucuronides [16]. Alternatively, X14 or X18 may be hemiacetal formation as reported by Wohlfarth *et al*. [16]. Carboxylation followed by hydroxylation (*m/z* 376, X10) showed the fragments at *m/z* 144 and 248 indicating hydroxylation at the fluoropentyl side chain.

A metabolite with oxidative defluorination (*m/z* 328, X25) was characterised by the fragment ions at *m/z* 125, 144 and 230 indicating a hydroxylated pentyl side chain. Hydroxylation of X25 led to X2 and X7 (*m/z* 344) with the fragment ions at *m/z* 144 and 230 suggesting hydroxylation at the TMCP ring. Further oxidation of X2 or X7 formed an aldehyde metabolite (*m/z* 342, X16) and a carboxylated metabolite (*m/z* 358, X8) both with the fragment ions at *m/z* 144 and 230. Oxidative defluorination to carboxylic acid (*m/z* 342, X24) was indicated by the fragment ions at *m/z* 125, 144 and 244. X24 was subsequently hydroxylated at the TMCP ring (*m/z* 358, X1, X4), further oxidated to aldehyde (*m/z* 356, X15, X17) and carboxylic acid (*m/z* 372, X5) all with the fragment ions at *m/z* 144 and 244. Notably, if the two metabolites at *m/z* 356 (X15 and X17) are aldehydes as tentatively assigned, it would be the only case where the (*E*)- and (*Z*)-isomers are not coeluted. Therefore, it is possible that one of them is a metabolite that underwent dihydroxylation followed by internal dehydration as previously reported [16].

UR-144

UR-144 is a defluorinated analogue of XLR-11. Hence, it showed the same fragment ions at *m/z* 125, 144 and the defluorinated ion at *m/z* 214, instead of 232 (**Fig. 1**). Hydroxylation (*m/z* 328) of UR-144 occurred at the pentyl side chain with the fragment ions at *m/z* 125, 144 and 230 (U22, U23) and at the TMCP ring with the ions at 144 and 214 (U24, U25). U22 matched well in retention time with X25 (oxidative defluorination metabolite of XLR-11), suggesting 5-hydroxypentyl metabolite. The position of hydroxylation for U23 cannot be determined but is likely to be 4-hydroxypentyl metabolite since (ω)-OH and (ω-1)-OH metabolites of alkyl side chain have been reported for some synthetic cannabinoids [33, 44]. Further hydroxylation of hydroxy metabolites resulted in dihydroxylation (*m/z* 344, U7, U11, U13, U16) with one hydroxy group at the pentyl side chain and another at the TMCP ring as indicated by the fragment ions at *m/z* 144 and 230 (**Fig. 1**). U7 and U11 agreed well with X2 and X7, respectively, indicating that the hydroxy group at the side chain is likely to be at the terminal carbon. Trihydroxylated metabolites (*m/z* 360, U1-U3, U5) were then formed with a hydroxy group at the pentyl side chain and two at the TMCP ring as shown by the fragment ions at *m/z* 144 and 230. *N*-dealkylation of U24 and U25 resulted in despentyl hydroxy metabolites (*m/z* 258, U4, U9) with the fragment ion at *m/z* 144.

Aldehyde formation at the TMCP ring followed by hydroxylation at the pentyl side chain (*m/z* 342, U19) was suggested by the fragment ions at *m/z* 144 and 230. Due to the close retention time with X16 (oxidative defluorination metabolite of XLR-11), U19 is likely to be hydroxylated at the 5-position of the pentyl side chain. Aldehyde at the TMCP ring followed by ketone at the pentyl side chain (*m/z* 340, U21) showed the fragment ions at the *m/z* 144 and 228 representing ketone formation at the pentyl side chain. Carboxylation at the pentyl side chain with hydroxylation at the TMCP ring (*m/z* 358, U6, U8) was suggested by the ions at *m/z* 144 and 244 indicative of *N*-pentanoic acid, which was supported by the matching retention time with X1 and X4, respectively. Similarly, carboxylation at the TMCP ring with

hydroxylation at the pentyl side chain (*m/z* 358, U10, U12, U15) was indicated by the ions at *m/z* 144 and 230. U10 was considered to be the same metabolite as X8 and is expected to have been hydroxylated at the terminal carbon.

Ketone formation at the pentyl side chain with hydroxylation at the TMCP ring (*m/z* 342, U14, U18) was suggested by the fragment ions at *m/z* 144 and 228. Ketone at the pentyl side chain with carboxylation at the TMCP ring (*m/z* 345, U17, U20) was represented by the fragment ions at *m/z* 144 and 228.

Comparison of fungal metabolites with reported human metabolites

For 5F-PB-22 and PB-22, the fungal metabolites were generally in good agreement with reported human *in vitro* metabolites (**Tables 1 and 2**). Almost all types of individual biotransformations reported for the human metabolism were observed for the fungal metabolism though not necessarily in the same combinations; the only transformations that lacked with the fungus were cysteine conjugation and glucuronidation. The important difference, however, was that ester hydrolysis that forms 5F-PI-COOH/PI-COOH was the main pathway found by human hepatocytes [17] and HLM [22] while it was not a major pathway for *C. elegans*. In hepatocytes, three out of the five most abundant 5F-PB-22 metabolites are ester hydrolysis products with/without hydroxylation or glucuronidation whereas all seven major metabolites of PB-22 are ester hydrolysis products with/without hydroxylation, ketone formation and/or glucuronidation [17]. In contrast, all the fungal metabolites with ester hydrolysis were among the minor metabolites. However, it should be noted that metabolites generated by *in vitro* models like hepatocytes and HLM are not always consistent with human urinary metabolites. Accordingly, it would have been ideal to compare the fungal metabolites directly with human urinary metabolites, but unfortunately such data was unavailable.

The majority of the human metabolites for XLR-11 and UR-144 were observed in the fungus samples (**Tables 3 and 4**). For XLR-11, hemiacetal, *N*-dealkylation, dehydration, hemiketal, trihydroxylation and glucuronidation were the only individual transformations found in both *in vivo* and *in vitro* human metabolism that were not generated by the fungus. The major human urine metabolites have been reported to be oxidative defluorination and oxidative defluorination to carboxylic acid with/without hydroxylation [45, 46], mostly of the pyrolysis product formed from thermal degradation due to smoking. All these metabolites were found in the fungus culture, though not of the pyrolysis product as the process of heating was not involved in this study, and metabolites with oxidative defluorination to carboxylic acid with hydroxylation (X1 and X4) were the fourth and fifth abundant fungal metabolites among 26 metabolites indicating good correlation in abundance. With UR-144, although metabolites with aldehyde, carboxylation, ketone or *N*-dealkylation alone were absent, all the reported human biotransformations including the four aforementioned were detected in fungal metabolism. Hydroxylation and dihydroxylation are reported major human urine metabolites [6, 47] and two dihydroxylated metabolites (U7 and U11) were found to be the two most abundant fungal metabolites.

These findings demonstrate that *C. elegans* is capable of most biotransformations observed for the four synthetic cannabinoids in humans, which is consistent with the previous studies

on JWH-018, JWH-073 and AM2201 [33]. Hence, it shows the potential to be used to predict metabolism of future cannabinoids, complementary to other models, and to characterise metabolites by NMR analysis. However, two distinct differences between the fungus and human metabolism seem to exist. One is that glucuronides were not observed in this study and instead glucosides were generated by the fungus. This finding agrees with the study on the synthetic cannabinoid AM2201 that glucosidation and sulfation are the only phase II reactions observed for *C. elegans* metabolism while glucuronidation is the major phase II transformation in humans [33]. Similarly, for some other drugs, glucosidation and sulfation are reported to be the phase II reactions of *C. elegans* while the same drugs are glucuronidated and sulfated in humans [38, 48]. The latter experiments did not involve extraction step as a sample preparation, supporting that poor recovery of glucuronides in dichloromethane is not likely a reason for the absence of glucuronides in this study. Furthermore, the retention time of the glucosides observed in this study were between 6-10 min. If glucuronides of corresponding aglycones were present in the culture, they would likely have been extracted by dichloromethane, which did extract polar compounds derived from matrix eluting between 3-6 min. This indicates that phase II metabolites produced by the fungus, particularly glucosides, may be irrelevant and need to be interpreted with caution, if hydrolysis step is not included in sample preparation before urinalysis. The other difference is that ester hydrolysis was clearly not a favoured pathway in the fungal metabolism. Previously, incubation of steroidal drug, ethynodiol diacetate containing two ester groups, with *C. elegans* and *Ocimum basilicum* has been reported [49] and while ester hydrolysis did not occur with *C. elegans*, three of the four metabolites by *Ocimum basilicum* underwent hydrolysis suggesting that *C. elegans* may not favour ester hydrolysis in general. Some of the other discrepancy between the fungus and human metabolites may be due to dosages, possible co-administration of drugs in authentic human samples, incubation/sampling time. Finally, there are limitations of the comparison method. Each biotransformation observed for fungus and human metabolism was compared in this study. While this method provides useful information on the major metabolic pathways, specific isomers found in fungal metabolism may not always be the exact isomers found in human metabolism, e.g. 2-pentylhydroxy isomer in fungus vs. 4-pentylhydroxy isomer in human urine. This limitation is inherent to the mass spectrometry technique used and highlights the need to use other complimentary techniques such as NMR to aid unambiguous structural elucidation of metabolites and to facilitate more accurate comparison.

Comparison of fungal model with in vitro human models

One of the incentives to use the fungus is the cost efficiency of the model. Unlike human hepatocytes or HLM, fungus can be repeatedly subcultured as required for new experiments. Therefore, once the stock culture of the fungus is obtained, potato dextrose agar plates for subculturing will essentially be the only cost associated for the subsequent use of fungus.

Regarding extrapolation of metabolic profiles to human metabolism, human hepatocytes appear to best serve the purpose as the biotransformations observed are most closely aligned to human metabolites including the phase II metabolites as observed for XLR-11 (**Table 3**) and the metabolite abundance is often closer to *in vivo* human metabolites [8]. While *C. elegans* did not match the human metabolites for XLR-11 as well as hepatocytes, it seems

just as useful as HLM, generating most of the HLM metabolites in addition to those not produced by HLM (**Tables 1-4**).

As previously mentioned, the fungus metabolism can be scaled up to produce amounts of metabolites sufficient for NMR analysis. This is useful because it allows for more definitive characterisation of metabolites. Metabolites/isomers found in human urine and *in vitro* studies are not always conclusively characterised since commercially available reference standards do not cover all the potential metabolites and isomers. With upscaling of fungus metabolism followed by NMR analysis, the obtained metabolites could act as reference standards and in conjunction with human metabolism studies, appropriate biomarkers can be suggested. The quantity of drugs and volume of the media required for upscaling will depend on how much drug is metabolised, how many metabolites are to be analysed, abundance of major metabolites among all the metabolites, recovery of the metabolites in extraction and sensitivity of NMR spectrometer. In this study, these parameters were not quantified, and consequently it is difficult to estimate the quantity and volume required. Previous studies report that as little as 0.9 mg of 18-nor-oxandrolone in 30 mL of media is sufficient for analysis of two metabolites [39] while five metabolites of adrenosterone were generated from 450 mg in 3 L, indicating the variability of the quantity and volume from case to case.

Conclusion

Metabolism of four synthetic cannabinoids, 5F-PB-22, XLR-11 and their defluorinated analogues PB-22 and UR-144 respectively, were investigated using the fungus *C. elegans*. The phase I and II metabolites were identified based on LC-QTOF analysis and their metabolic pathways were proposed. Hydroxylation, dihydroxylation, dihydrodiol formation, oxidative defluorination, oxidative defluorination to carboxylic acid, ester hydrolysis, glucosidation and combinations of these were observed for 5F-PB-22 with some of them only appearing as combinations. For PB-22, transformations were similar, but trihydroxylation, ketone formation and carboxylation were found instead of oxidative defluorination (to carboxylic acid). XLR-11 underwent hydroxylation, dihydroxylation, aldehyde formation, carboxylation, oxidative defluorination, oxidative defluorination to carboxylic acid and glucosidation either alone or in combinations. With UR-144, trihydroxylation, ketone formation and *N*-dealkylation were observed instead of oxidative defluorination (to carboxylic acid) and glucosidation. Comparison of the fungal metabolites with reported human metabolites showed that while *C. elegans* has limitations, such as low abundance of ester hydrolysis and absence of glucuronidation, overall the metabolic profiles were in good agreement. Therefore, it might have the potential to be a complementary model for synthetic cannabinoid metabolism.

Conflicts of interest

None.

References

1. European Monitoring Centre for Drugs and Drug Addiction. European Drug Report 2016: Trends and Developments. Luxembourg: Publications Office of the European Union 2016.
2. Chimalakonda KC, Seely KA, Bratton SM, Brents LK, Moran CL, Endres GW, et al. Cytochrome P450-mediated oxidative metabolism of abused synthetic cannabinoids found in K2/Spice: identification of novel cannabinoid receptor ligands. Drug Metab Dispos. 2012;40(11):2174-84. doi:10.1124/dmd.112.047530.
3. Fantegrossi WE, Moran JH, Radominska-Pandya A, Prather PL. Distinct pharmacology and metabolism of K2 synthetic cannabinoids compared to Delta(9)-THC: mechanism underlying greater toxicity? Life Sci. 2014;97(1):45-54. doi:10.1016/j.lfs.2013.09.017.
4. Trecki J, Gerona RR, Schwartz MD. Synthetic Cannabinoid–Related Illnesses and Deaths. N Engl J Med. 2015;373(2):103-7. doi:doi:10.1056/NEJMp1505328.
5. Grigoryev A, Savchuk S, Melnik A, Moskaleva N, Dzhurko J, Ershov M, et al. Chromatography-mass spectrometry studies on the metabolism of synthetic cannabinoids JWH-018 and JWH-073, psychoactive components of smoking mixtures. J Chromatogr B. 2011;879(15-16):1126-36. doi:10.1016/j.jchromb.2011.03.034.
6. Sobolevsky T, Prasolov I, Rodchenkov G. Detection of urinary metabolites of AM-2201 and UR-144, two novel synthetic cannabinoids. Drug Test Anal. 2012;4(10):745-53. doi:10.1002/dta.1418.
7. Wohlfarth A, Castaneto MS, Zhu M, Pang S, Scheidweiler KB, Kronstrand R, et al. Pentylindole/Pentylindazole Synthetic Cannabinoids and Their 5-Fluoro Analogs Produce Different Primary Metabolites: Metabolite Profiling for AB-PINACA and 5F-AB-PINACA. AAPS J. 2015;17(3):660-77. doi:10.1208/s12248-015-9721-0.
8. Diao X, Scheidweiler KB, Wohlfarth A, Pang S, Kronstrand R, Huestis MA. In Vitro and In Vivo Human Metabolism of Synthetic Cannabinoids FDU-PB-22 and FUB-PB-22. AAPS J. 2016;18(2):455-64. doi:10.1208/s12248-016-9867-4.
9. Castaneto MS, Wohlfarth A, Pang S, Zhu M, Scheidweiler KB, Kronstrand R, et al. Identification of AB-FUBINACA metabolites in human hepatocytes and urine using high-resolution mass spectrometry. Forensic Toxicol. 2015;33(2):295-310. doi:10.1007/s11419-015-0275-8.
10. Vikingsson S, Green H, Brinkhagen L, Mukhtar S, Josefsson M. Identification of AB-FUBINACA metabolites in authentic urine samples suitable as urinary markers of drug intake using liquid chromatography quadrupole tandem time of flight mass spectrometry. Drug Test Anal. 2016;8(9):950-6. doi:10.1002/dta.1896.
11. Sobolevsky T, Prasolov I, Rodchenkov G. Detection of JWH-018 metabolites in smoking mixture post-administration urine. Forensic Sci Int. 2010;200(1-3):141-7. doi:10.1016/j.forsciint.2010.04.003.
12. Kavanagh P, Grigoryev A, Melnik A, Savchuk S, Simonov A, Rozhanets V. Detection and tentative identification of urinary phase I metabolites of phenylacetylindole cannabimimetics JWH-203 and JWH-251, by GC–MS and LC–MS/MS. J Chromatogr B. 2013;934:102-8. doi:http://dx.doi.org/10.1016/j.jchromb.2013.07.005.
13. Zaitsu K, Nakayama H, Yamanaka M, Hisatsune K, Taki K, Asano T, et al. High-resolution mass spectrometric determination of the synthetic cannabinoids MAM-2201, AM-2201, AM-2232, and their metabolites in postmortem plasma and urine by LC/Q-TOFMS. Int J Legal Med. 2015;129(6):1233-45. doi:10.1007/s00414-015-1257-4.
14. Sobolevsky T, Prasolov I, Rodchenkov G. Study on the phase I metabolism of novel synthetic cannabinoids, APICA and its fluorinated analogue. Drug Test Anal. 2015;7(2):131-42. doi:10.1002/dta.1756.
15. Hutter M, Moosmann B, Kneisel S, Auwarter V. Characteristics of the designer drug and synthetic cannabinoid receptor agonist AM-2201 regarding its chemistry and metabolism. J Mass Spectrom. 2013;48(7):885-94. doi:10.1002/jms.3229.

16. Wohlfarth A, Pang S, Zhu M, Gandhi AS, Scheidweiler KB, Liu HF, et al. First metabolic profile of XLR-11, a novel synthetic cannabinoid, obtained by using human hepatocytes and high-resolution mass spectrometry. Clin Chem. 2013;59(11):1638-48. doi:10.1373/clinchem.2013.209965.
17. Wohlfarth A, Gandhi AS, Pang S, Zhu M, Scheidweiler KB, Huestis MA. Metabolism of synthetic cannabinoids PB-22 and its 5-fluoro analog, 5F-PB-22, by human hepatocyte incubation and high-resolution mass spectrometry. Anal Bioanal Chem. 2014;406(6):1763-80. doi:10.1007/s00216-014-7668-0.
18. Diao X, Scheidweiler KB, Wohlfarth A, Zhu M, Pang S, Huestis MA. Strategies to distinguish new synthetic cannabinoid FUBIMINA (BIM-2201) intake from its isomer THJ-2201: metabolism of FUBIMINA in human hepatocytes. Forensic Toxicol. 2016;34:256-67. doi:10.1007/s11419-016-0312-2.
19. Diao X, Wohlfarth A, Pang S, Scheidweiler KB, Huestis MA. High-Resolution Mass Spectrometry for Characterizing the Metabolism of Synthetic Cannabinoid THJ-018 and Its 5-Fluoro Analog THJ-2201 after Incubation in Human Hepatocytes. Clin Chem. 2016;62(1):157-69. doi:10.1373/clinchem.2015.243535.
20. Gandhi AS, Zhu M, Pang S, Wohlfarth A, Scheidweiler KB, Liu HF, et al. First characterization of AKB-48 metabolism, a novel synthetic cannabinoid, using human hepatocytes and high-resolution mass spectrometry. AAPS J. 2013;15(4):1091-8. doi:10.1208/s12248-013-9516-0.
21. Wintermeyer A, Moller I, Thevis M, Jubner M, Beike J, Rothschild MA, et al. In vitro phase I metabolism of the synthetic cannabimimetic JWH-018. Anal Bioanal Chem. 2010;398(5):2141-53. doi:10.1007/s00216-010-4171-0.
22. Takayama T, Suzuki M, Todoroki K, Inoue K, Min JZ, Kikura-Hanajiri R, et al. UPLC/ESI-MS/MS-based determination of metabolism of several new illicit drugs, ADB-FUBINACA, AB-FUBINACA, AB-PINACA, QUPIC, 5F-QUPIC and alpha-PVT, by human liver microsome. Biomed Chromatogr. 2014;28(6):831-8. doi:10.1002/bmc.3155.
23. Jang M, Shin I, Yang W, Chang H, Yoo HH, Lee J, et al. Determination of major metabolites of MAM-2201 and JWH-122 in in vitro and in vivo studies to distinguish their intake. Forensic Sci Int. 2014;244:85-91. doi:10.1016/j.forsciint.2014.08.008.
24. Vikingsson S, Josefsson M, Green H. Identification of AKB-48 and 5F-AKB-48 Metabolites in Authentic Human Urine Samples Using Human Liver Microsomes and Time of Flight Mass Spectrometry. J Anal Toxicol. 2015;39(6):426-35. doi:10.1093/jat/bkv045.
25. De Brabanter N, Esposito S, Geldof L, Lootens L, Meuleman P, Leroux-Roels G, et al. In vitro and in vivo metabolisms of 1-pentyl-3-(4-methyl-1-naphthoyl)indole (JWH-122). Forensic Toxicol. 2013;31(2):212-22. doi:10.1007/s11419-013-0179-4.
26. De Brabanter N, Esposito S, Tudela E, Lootens L, Meuleman P, Leroux-Roels G, et al. In vivo and in vitro metabolism of the synthetic cannabinoid JWH-200. Rapid Commun Mass Spectrom. 2013;27(18):2115-26. doi:10.1002/rcm.6673.
27. Schaefer N, Helfer AG, Kettner M, Laschke MW, Schlote J, Ewald AH, et al. Metabolic patterns of JWH-210, RCS-4, and THC in pig urine elucidated using LC-HR-MS/MS: Do they reflect patterns in humans? Drug Test Anal. 2016. doi:10.1002/dta.1995.
28. Maurer HH, Meyer MR. High-resolution mass spectrometry in toxicology: current status and future perspectives. Arch Toxicol. 2016;90(9):2161-72. doi:10.1007/s00204-016-1764-1.
29. Diao X, Huestis MA. Approaches, Challenges, and Advances in Metabolism of New Synthetic Cannabinoids and Identification of Optimal Urinary Marker Metabolites. Clin Pharmacol Ther. 2017;101(2):239-53. doi:10.1002/cpt.534.
30. Asha S, Vidyavathi M. Cunninghamella--a microbial model for drug metabolism studies--a review. Biotechnol Adv. 2009;27(1):16-29. doi:10.1016/j.biotechadv.2008.07.005.
31. Zhang D, Yang Y, Leakey JEA, Cerniglia CE. Phase I and phase II enzymes produced by Cunninghamella elegans for the metabolism of xenobiotics. FEMS Microbiol Lett. 1996;138(2-3):221-6. doi:10.1111/j.1574-6968.1996.tb08161.x.

32. Wang R-F, Cao W-W, Khan AA, Cerniglia CE. Cloning, sequencing, and expression in Escherichia coli of a cytochrome P450 gene from Cunninghamella elegans. FEMS Microbiol Lett. 2000;188(1):55-61. doi:10.1111/j.1574-6968.2000.tb09168.x.
33. Watanabe S, Kuzhiumparambil U, Winiarski Z, Fu S. Biotransformation of synthetic cannabinoids JWH-018, JWH-073 and AM2201 by Cunninghamella elegans. Forensic Sci Int. 2016;261:33-42. doi:http://dx.doi.org/10.1016/j.forsciint.2015.12.023.
34. Kaminsky LS, Zhang Z-Y. Human P450 metabolism of warfarin. Pharmacol Ther. 1997;73(1):67-74. doi:http://dx.doi.org/10.1016/S0163-7258(96)00140-4.
35. Wong YWJ, Davis PJ. Microbial Models of Mammalian Metabolism: Stereoselective Metabolism of Warfarin in the Fungus Cunninghamella elegans. Pharm Res. 1989;6(11):982-7. doi:10.1023/a:1015905832184.
36. Olesen OV, Linnet K. Metabolism of the Tricyclic Antidepressant Amitriptyline by cDNA-Expressed Human Cytochrome P450 Enzymes. Pharmacology. 1997;55(5):235-43. doi:10.1159/000139533.
37. Zhang D, Evans FE, Freeman JP, Duhart B, Cerniglia CE. Biotransformation of amitriptyline by Cunninghamella elegans. Drug Metab Dispos. 1995;23(12):1417-25.
38. Hansson A, Thevis M, Cox H, Miller G, Eichner D, Bondesson U, et al. Investigation of the metabolites of the HIF stabilizer FG-4592 (roxadustat) in five different in vitro models and in a human doping control sample using high resolution mass spectrometry. J Pharm Biomed Anal. 2017;134:228-36. doi:10.1016/j.jpba.2016.11.041.
39. Guddat S, Fußhöller G, Beuck S, Thomas A, Geyer H, Rydevik A, et al. Synthesis, characterization, and detection of new oxandrolone metabolites as long-term markers in sports drug testing. Anal Bioanal Chem. 2013;405(25):8285-94. doi:10.1007/s00216-013-7218-1.
40. Tian J-L, Chen Y, Wang Y-X, Huang X-X, Sun X, Liu K-C, et al. Microbial transformation of methyl cyperenoate by Cunninghamella elegans AS 3.2028 and the antithrombotic activities of its metabolites. RSC Adv. 2016;6(113):112712-20. doi:10.1039/c6ra24332k.
41. Watanabe S, Kuzhiumparambil U, Winiarski Z, Fu S. Data on individual metabolites of synthetic cannabinoids JWH-018, JWH-073 and AM2201 by Cunninghamella elegans. Data Brief. 2016;7:332-40. doi:10.1016/j.dib.2016.02.039.
42. Choudhary MI, Khan NT, Musharraf SG, Anjum S, Atta ur R. Biotransformation of adrenosterone by filamentous fungus, Cunninghamella elegans. Steroids. 2007;72(14):923-9. doi:http://dx.doi.org/10.1016/j.steroids.2007.08.002.
43. Schwartz H, Liebig-Weber A, Hochstätter H, Böttcher H. Microbial oxidation of ebastine. Appl Microbiol Biotechnol. 1996;44(6):731-5. doi:10.1007/bf00178610.
44. Chimalakonda KC, Moran CL, Kennedy PD, Endres GW, Uzieblo A, Dobrowolski PJ, et al. Solid-phase extraction and quantitative measurement of omega and omega-1 metabolites of JWH-018 and JWH-073 in human urine. Anal Chem. 2011;83(16):6381-8. doi:10.1021/ac201377m.
45. Kanamori T, Kanda K, Yamamuro T, Kuwayama K, Tsujikawa K, Iwata YT, et al. Detection of main metabolites of XLR-11 and its thermal degradation product in human hepatoma HepaRG cells and human urine. Drug Test Anal. 2015;7(4):341-5. doi:10.1002/dta.1765.
46. Jang M, Kim IS, Park YN, Kim J, Han I, Baeck S, et al. Determination of urinary metabolites of XLR-11 by liquid chromatography-quadrupole time-of-flight mass spectrometry. Anal Bioanal Chem. 2016;408(2):503-16. doi:10.1007/s00216-015-9116-1.
47. Grigoryev A, Kavanagh P, Melnik A, Savchuk S, Simonov A. Gas and liquid chromatography-mass spectrometry detection of the urinary metabolites of UR-144 and its major pyrolysis product. J Anal Toxicol. 2013;37(5):265-76. doi:10.1093/jat/bkt028.
48. Rydevik A, Thevis M, Krug O, Bondesson U, Hedeland M. The fungus Cunninghamella elegans can produce human and equine metabolites of selective androgen receptor modulators (SARMs). Xenobiotica. 2013;43(5):409-20. doi:10.3109/00498254.2012.729102.

49. Zafar S, Yousuf S, Kayani HA, Saifullah S, Khan S, Al-Majid AM, et al. Biotransformation of oral contraceptive ethynodiol diacetate with microbial and plant cell cultures. Chem Cent J. 2012;6(1):109. doi:10.1186/1752-153x-6-109.
50. Nielsen LM, Holm NB, Olsen L, Linnet K. Cytochrome P450-mediated metabolism of the synthetic cannabinoids UR-144 and XLR-11. Drug Test Anal. 2016;8(8):792-800. doi:10.1002/dta.1860.
51. Scheidweiler KB, Jarvis MJ, Huestis MA. Nontargeted SWATH acquisition for identifying 47 synthetic cannabinoid metabolites in human urine by liquid chromatography-high-resolution tandem mass spectrometry. Anal Bioanal Chem. 2015;407(3):883-97. doi:10.1007/s00216-014-8118-8.
52. Park M, Yeon S, Lee J, In S. Determination of XLR-11 and its metabolites in hair by liquid chromatography-tandem mass spectrometry. J Pharm Biomed Anal. 2015;114:184-9. doi:10.1016/j.jpba.2015.05.022.
53. Adamowicz P, Zuba D, Sekula K. Analysis of UR-144 and its pyrolysis product in blood and their metabolites in urine. Forensic Sci Int. 2013;233(1-3):320-7. doi:10.1016/j.forsciint.2013.10.005.

Figures

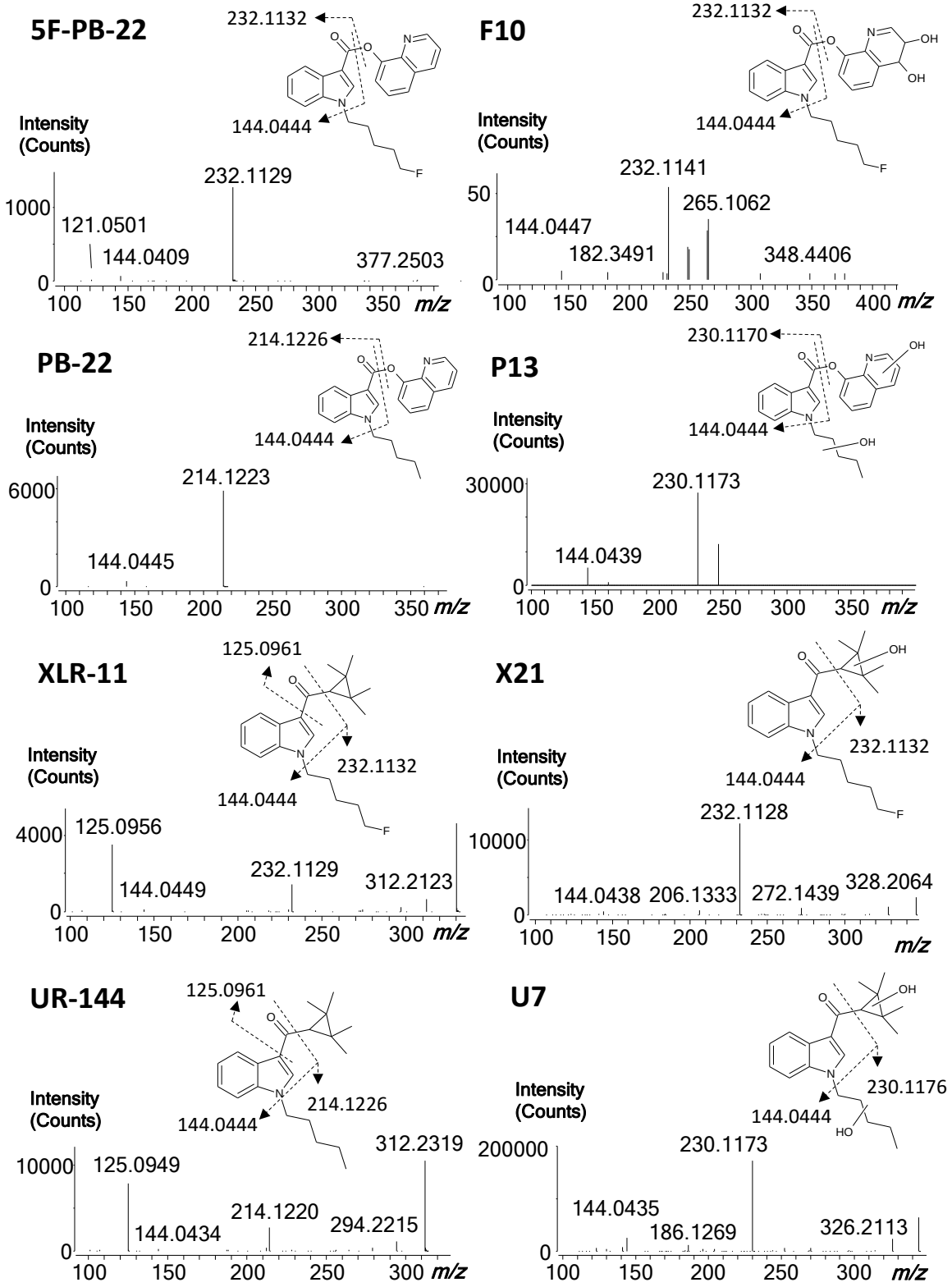

Fig. 1. MS/MS spectra obtained with CE 20 eV and structures with the suggested fragmentation patterns and their exact masses for the parent drugs (5F-PB-22, PB-22, XLR-11 and UR-144) and their most abundant fungal metabolites based on peak area (F10, P13, X21 and U7). The exact position of the dihydrodiol structure within quinolone moiety in F10 is not determined.

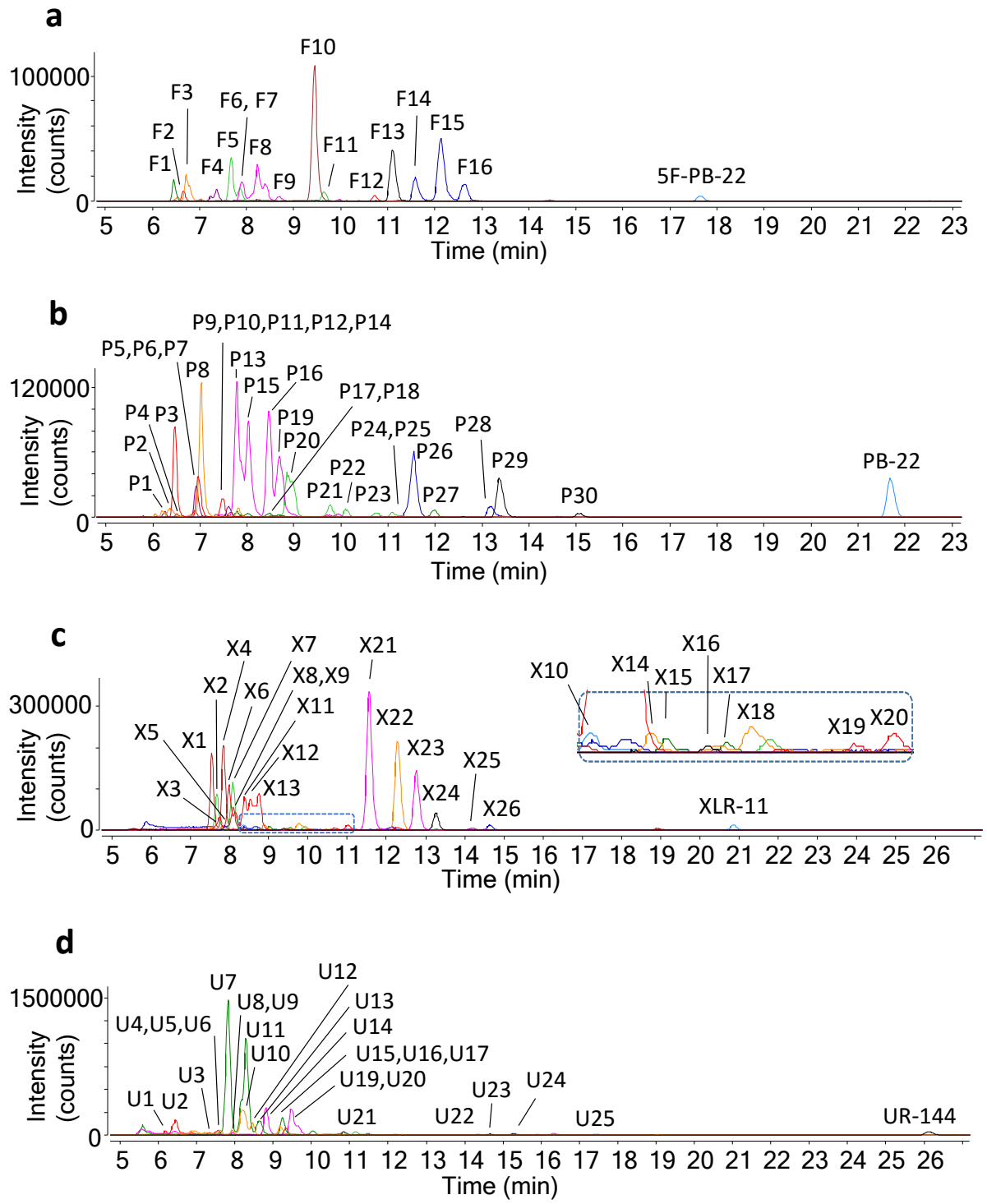

Fig. 2. Combined extracted ion chromatograms of all metabolites and their respective parent drugs for (**a)** 5F-PB-22, (**b)** PB-22, (**c**) XLR-11, and (**d)** UR-144 after incubation with *C. elegans*.

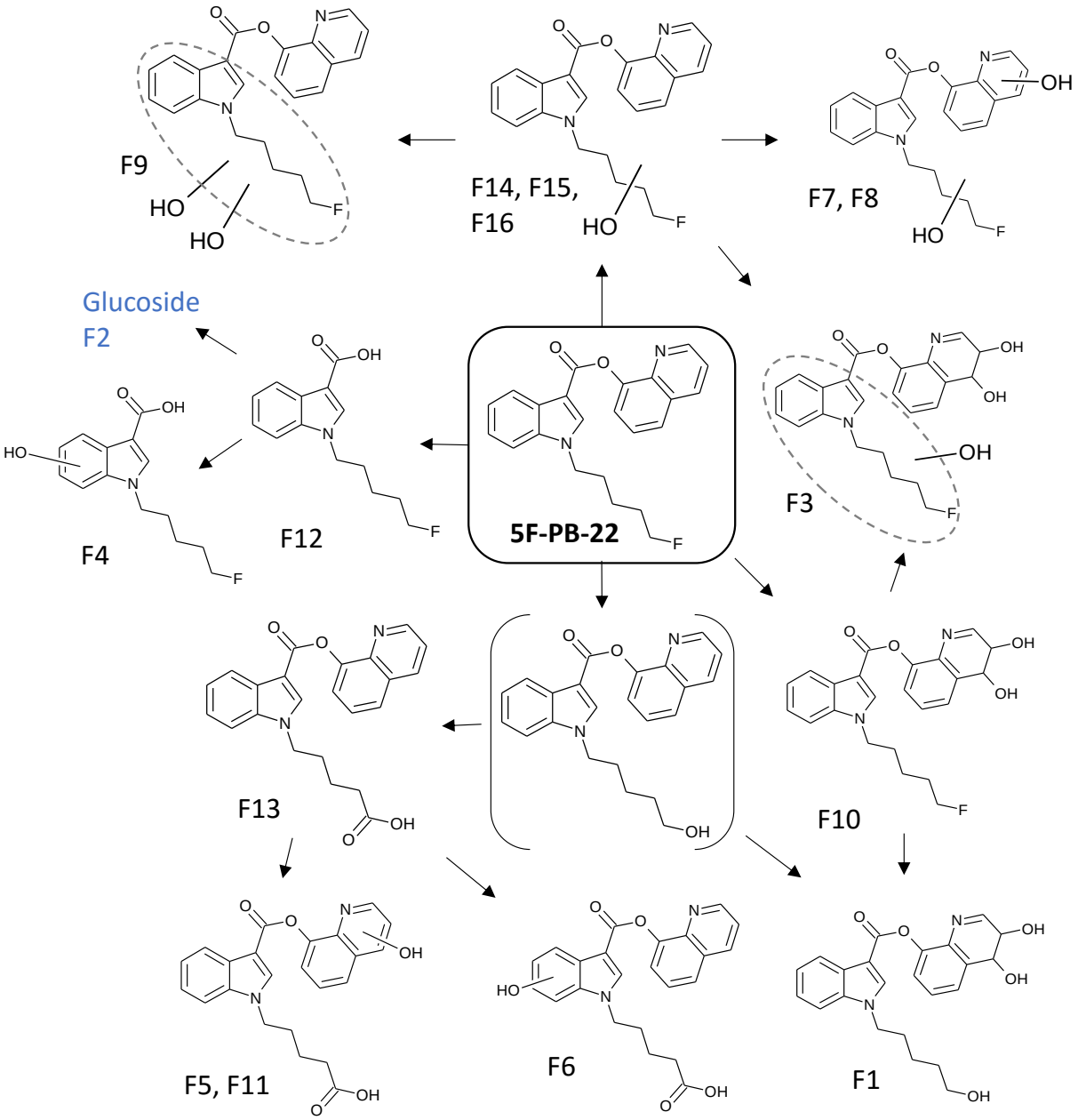

Fig. 3. Proposed metabolic pathway of 5F-PB-22 by *C. elegans*. Blue colour denotes a Phase II metabolite. Parenthesis represents a possible intermediate metabolite that was not detected in the study. For the metabolites with dihydrodiol structure, only one possible isomer is shown as a representative.

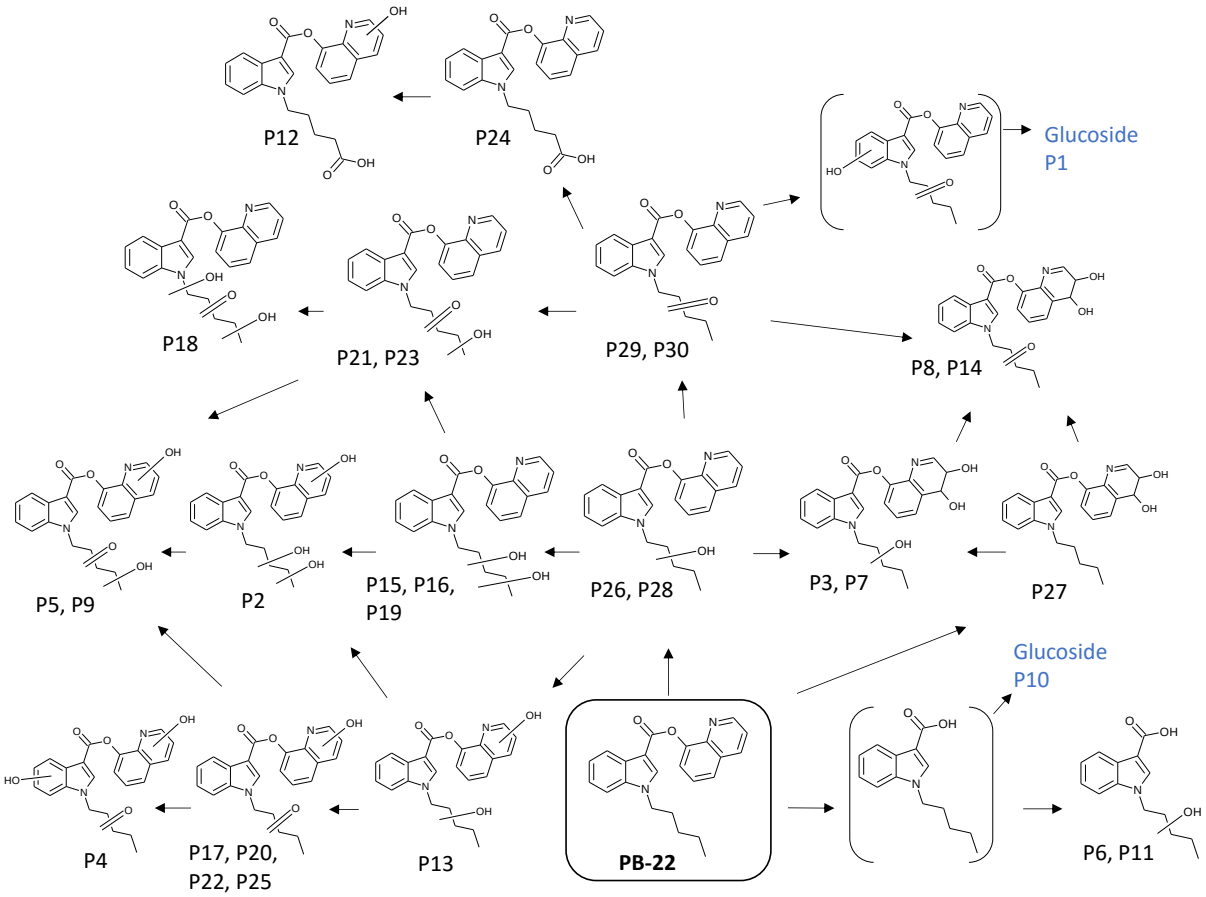

Fig. 4. Proposed metabolic pathway of PB-22 by *C. elegans*. Blue colour denotes Phase II metabolites. Parentheses represent possible intermediate metabolites that were not detected in the study. For the metabolites with dihydrodiol structure, only one possible isomer is shown as a representative.

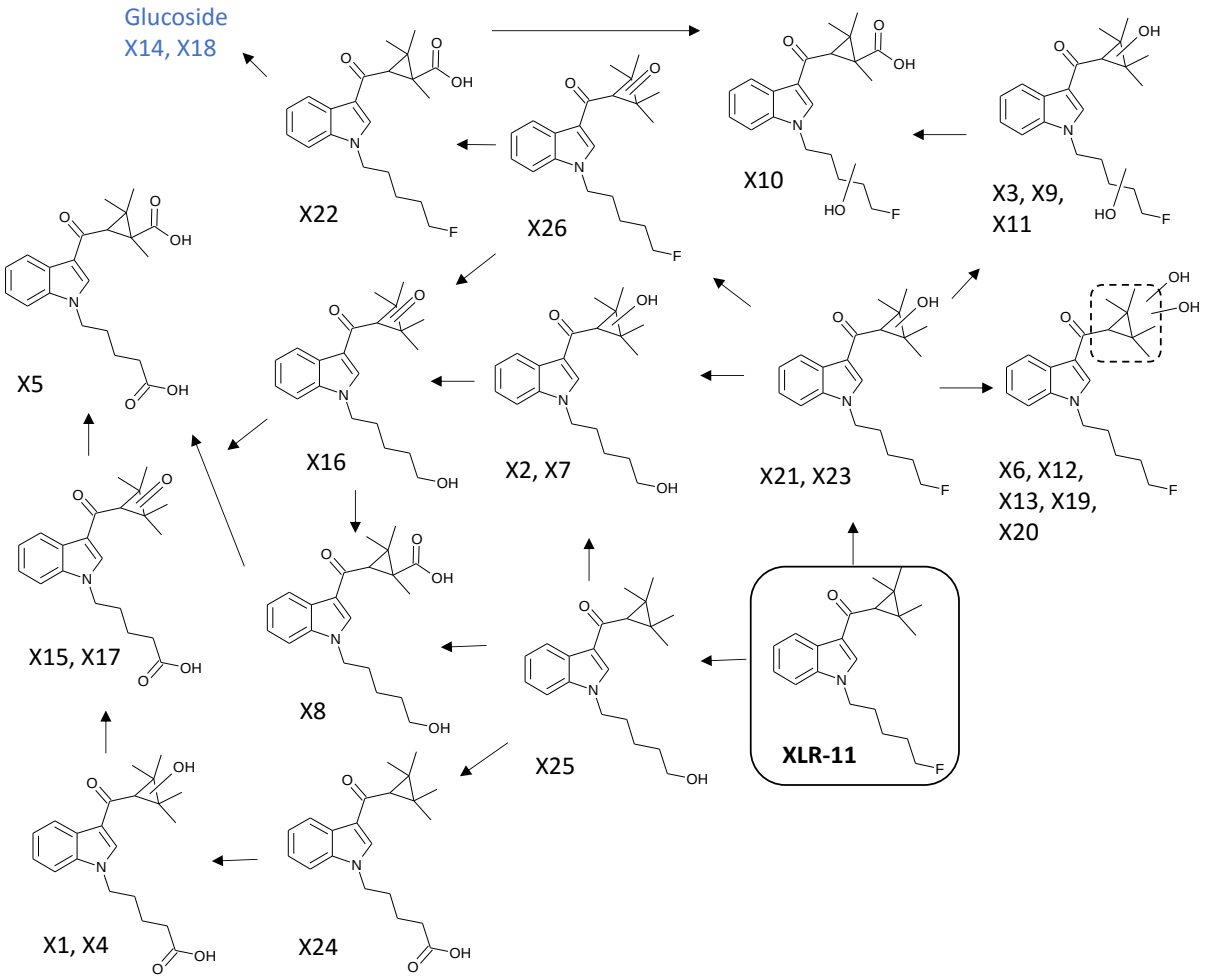

Fig. 5. Proposed metabolic pathway of XLR-11 by *C. elegans*. Blue colour denotes Phase II metabolites.

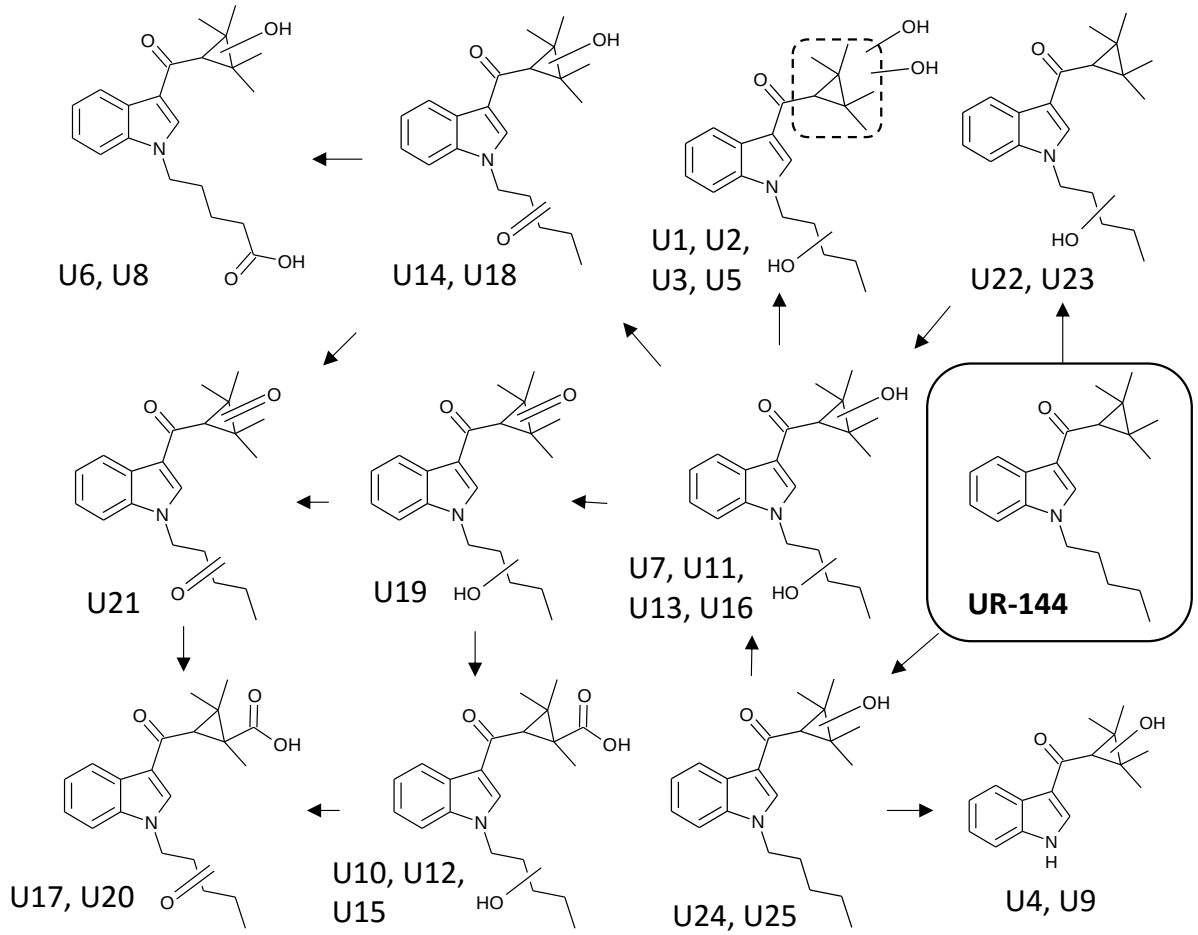

Fig. 6. Proposed metabolic pathway of UR-144 by *C. elegans*.

Tables

Table I. Comparison of 5F-PB-22 metabolites formed by fungus, *Cunninghamella elegans*, with those by human hepatocytes and human liver microsomes reported in literature.

Metabolites	CE	HHep	HLM
5F-PI-COOH [F12]	√	√ [17]	√ [22]
5F-PI-COOH + glucosidation [F2]	√		
5F-PI-COOH + glucuronidation		√ [17]	
5F-PI-COOH + cysteine conjugation		√ [17]	
5F-PI-COOH + hydroxylation [F4]	√	√ [17]	
5F-PI-COOH + hydroxylation + glucuronidation		√ [17]	
5F-PI-COOH + oxidative defluorination		√ [17]	
5F-PI-COOH + oxidative defluorination to carboxylic acid		√ [17]	
5F-PI-COOH + oxidative defluorination to carboxylic acid + glucuronidation		√ [17]	
Dihydrodiol formation [F10]	√	√ [17]	
Dihydrodiol formation + hydroxylation [F3]	√		
Dihydroxylation [F7-F9]	√		
Dihydroxylation + glucuronidation		√ [17]	
Hydroxylation [F14 - F16]	√	√ [17]	
Hydroxylation + glucuronidation		√ [17]	
Oxidative defluorination + dihydrodiol formation [F1]	√		
Oxidative defluorination + glucuronidation		√ [17]	
Oxidative defluorination to carboxylic acid [F13]	√	√ [17]	
Oxidative defluorination to carboxylic acid + glucuronidation		√ [17]	
Oxidative defluorination to carboxylic acid + hydroxylation [F5, F6, F11]	√		

CE Cunninghamella elegans; *HHep* Human hepatocytes; *HLM* Human liver microsomes

Square brackets in Metabolites column indicate the ID of corresponding fungal metabolites.

Phase II metabolites are shown in blue colour.

Table II. Comparison of PB-22 metabolites formed by fungus, *Cunninghamella elegans*, with those by human hepatocytes and human liver microsomes reported in literature.

Metabolites	**CE**	**HHep**	**HLM**
Carboxylation [P24]	√	√ [17]	
Carboxylation + hydroxylation [P12]	√		
Dihydrodiol formation [P27]	√	√ [17]	
Dihydrodiol formation + hydroxylation [P3, P7]	√		
Dihydrodiol formation + ketone formation [P8, P14]	√		
Dihydroxylation [P13, P15, P16, P19]	√		
Hydroxylation [P26, P28]	√	√ [17]	
Hydroxylation + glucuronidation		√ [17]	
Ketone formation [P29, P30]	√	√ [17]	
Ketone formation + dihydroxylation [P4, P5, P9, P18]	√		
Ketone formation + hydroxylation [P17, P20 - P23, P25]	√		
Ketone formation + hydroxylation + glucosidation [P1]	√		
PI-COOH		√ [17]	√ [22]
PI-COOH + glucosidation [P10]	√		
PI-COOH + glucuronidation		√ [17]	
PI-COOH + carboxylation + glucuronidation		√ [17]	
PI-COOH + cysteine conjugation		√ [17]	
PI-COOH + hydroxylation [P6, P11]	√	√ [17]	
PI-COOH + hydroxylation + glucuronidation		√ [17]	
PI-COOH + ketone formation + glucuronidation		√ [17]	
Trihydroxylation [P2]	√		

CE Cunninghamella elegans; *HHep* Human hepatocytes; *HLM* Human liver microsomes

Square brackets in Metabolites column indicate the ID of corresponding fungal metabolites.

Phase II metabolites are shown in blue colour.

Table III. Comparison of XLR-11 metabolites formed by fungus, *Cunninghamella elegans*, with those in human urine and human liver microsomes reported in literature.

Metabolites	CE	HU		HH	HHep	HLM	HRG	
		XLR-11	Pyrolysis product[a]				XLR-11	Pyrolysis product[a]
Aldehyde formation[b] [X26]	√				√ [16]	√ [50]		
Aldehyde formation + hydroxylation followed by hemiacetal formation + glucuronidation					√ [16]			
Carboxylation [X22]	√				√ [16]	√ [50]		
Carboxylation + glucosidation [X14, X18]	√							
Carboxylation + glucuronidation					√ [16]			
Carboxylation + hydroxylation [X10]	√				√ [16]			
Dihydroxylation [X3, X6, X9, X11-X13, X19, X20]	√		√ [45]				√ [45]	√ [45]
Dihydroxylation + glucuronidation		√ [46]	√ [46]		√ [16]			
Hydroxylation [X21, X23]	√	√ [51]	√ [45, 46]	√ [52]		√ [50]	√ [45]	√ [45]
Hydroxylation + glucuronidation					√ [16]			
N-dealkylation						√ [50]		
Oxidative defluorination [X25]	√	√ [45, 46]	√ [45]	√ [52]	√ [16]	√ [46, 50]	√ [45]	√ [45]
Oxidative defluorination + glucuronidation		√ [46]	√ [46]		√ [16]			
Oxidative defluorination + aldehyde formation[b] [X16]	√					√ [50]		
Oxidative defluorination + carboxylation [X8]	√				√ [16]	√ [50]		
Oxidative defluorination + hydroxylation [X2, X7]	√		√ [45]			√ [50]	√ [45]	√ [45]
Oxidative defluorination + hydroxylation + glucuronidation			√ [46]		√ [16]			
Oxidative defluorination to carboxylic acid [X24]	√	√ [45, 46]	√ [45, 46]	√ [52]	√ [16]	√ [46]	√ [45]	√ [45]
Oxidative defluorination to carboxylic acid + glucuronidation			√ [46]		√ [16]			
Oxidative defluorination to carboxylic acid + aldehyde formation[b] [X15, X17]	√				√ [16]			
Oxidative defluorination to carboxylic acid + aldehyde formation + hydroxylation followed by hemiacetal formation					√ [16]			
Oxidative defluorination to carboxylic acid + aldehyde formation + hydroxylation followed by hemiacetal formation + glucuronidation					√ [16]			
Oxidative defluorination to	√	√ [46]	√ [46]		√ [16]			

carboxylic acid + carboxylation [X5]						
Oxidative defluorination to carboxylic acid + carboxylation + glucuronidation				√ [16]		
Oxidative defluorination to carboxylic acid + hydroxylation [X1, X4]	√	√ [46]	√ [45, 46]	√ [16]	√ [45]	√ [45]
Oxidative defluorination to carboxylic acid + hydroxylation + dehydration		√ [46]	√ [46]			
Oxidative defluorination to carboxylic acid + hydroxylation + hemiketal formation				√ [16]		
Trihydroxylation + glucuronidation				√ [16]		

CE Cunninghamella elegans; *HU* Human urine; *HH* Human hair; *HHep* Human hepatocytes; *HLM* Human liver microsomes; *HRG* HepaRG cells

[a] Metabolites of XLR-11 pyrolysis product are shown separately from those of non-pyrolysed XLR-11.

[b] The biotransformation proposed as ‘dioxidation followed by internal dehydration’ in the reference is included since it might be the same biotransformation.

Square brackets in Metabolites column indicate the ID of corresponding fungal metabolites.

Phase II metabolites are shown in blue colour.

Table IV. Comparison of UR-144 metabolites formed by fungus, *Cunninghamella elegans*, with those in human urine and human liver microsomes reported in literature.

Metabolites	**CE**	**HU**		**HLM**
		UR-144	**Pyrolysis product[a]**	
Aldehyde formation[b]				√ [6, 50]
Aldehyde formation[b] + hydroxylation [U19]	√			√ [50]
Aldehyde formation + ketone formation [U21]	√			
Carboxylation		√ [51]	√ [47, 51, 53]	√ [50]
Carboxylation + hydroxylation [U6, U8, U10, U12, U15]	√			√ [50]
Dihydroxylation [U7, U11, U13, U16]	√	√ [6, 47, 53]	√ [47, 53]	√ [6, 50]
Hydroxylation [U22 – U25]	√	√ [6, 47, 51]	√ [47, 53]	√ [6, 50]
Ketone formation				√ [6]
Ketone formation + carboxylation [U17, U20]	√			
Ketone formation + hydroxylation [U14, U18]	√	√ [47]	√ [47]	
N-dealkylation		√ [6]		√ [6]
N-dealkylation + hydroxylation [U4, U9]	√	√ [47]	√ [47]	√ [6]
Trihydroxylation [U1 - U3, U5]	√			

CE Cunninghamella elegans; *HU* Human urine; *HLM* Human liver microsomes

[a] Metabolites of UR-144 pyrolysis product are shown separately from those of non-pyrolysed UR-144.

[b] The biotransformation proposed as ‘dioxidation followed by internal dehydration’ or ‘dehydrated hydroxy’ in the reference is included since they might be the same biotransformation.

Square brackets in Metabolites column indicate the ID of corresponding fungal metabolites.

Supplementary Table I

5F-PB-22 metabolites with retention time, elemental composition, exact mass, accurate mass, mass error and diagnostic product ions.

ID	Metabolites	RT (min)	Elemental composition [M+H]	Exact mass	Accurate mass	Mass error (ppm)	Diagnostic product ions
F1	Oxidative deluorination + dihydrodiol formation	6.4	C23H25N2O5	409.1758	409.1761	0.76	230
F2	5F-PI-COOH + glucosidation	6.6	C20H27FNO7	412.1766	412.1772	1.39	118, 132, 144, 206, 232, 250
F3	Dihydrodiol formation + hydroxylation	6.7	C23H24FN2O5	427.1664	427.1665	0.35	248
F4	5F-PI-COOH + hydroxylation	7.4	C14H17FNO3	266.1187	266.1191	1.12	134, 148, 174, 222, 248
F5	Oxidative defluorination to carboxylic acid + hydroxylation	7.7	C23H21N2O5	405.1445	405.1448	0.71	144, 244
F6	Oxidative defluorination to carboxylic acid + hydroxylation	7.9	C23H21N2O5	405.1445	405.1447	0.53	160, 260
F7	Dihydroxylation	7.9	C23H22FN2O4	409.1558	409.1560	0.52	144, 248
F8	Dihydroxylation	8.2	C23H22FN2O4	409.1558	409.1557	-0.36	144, 158, 248
F9	Dihydroxylation	8.7	C23H22FN2O4	409.1558	409.1561	0.77	264
F10	Dihydrodiol formation	9.4	C23H24FN2O4	411.1715	411.1715	0.09	144, 232
F11	Oxidative defluorination to carboxylic acid + hydroxylation	9.6	C23H21N2O5	405.1445	405.1449	0.91	144, 244
F12	5F-PI-COOH	10.7	C14H17FNO2	250.1238	250.1240	0.73	118, 132, 144, 206, 232

F13	Oxidative defluorination to carboxylic acid	11.1	C23H21N2O4	389.1496	389.1498	0.54	144, 244
F14	Hydroxylation	11.6	C23H22FN2O3	393.1609	393.1612	0.75	144, 248
F15	Hydroxylation	12.1	C23H22FN2O3	393.1609	393.1612	0.72	144, 158, 248
F16	Hydroxylation	12.6	C23H22FN2O3	393.1609	393.1610	0.32	144, 248
Parent	5F-PB-22	17.6	C23H22FN2O2	377.1660	377.1664	1.17	144, 232

Supplementary Table II

PB-22 metabolites with retention time, elemental composition, exact mass, accurate mass, mass error and diagnostic product ions.

ID	Metabolites	RT (min)	Elemental composition [M+H]	Exact mass	Accurate mass	Mass error (ppm)	Diagnostic product ions
P1	Ketone formation + hydroxylation + glucosidation	6.2	C29H31N2O9	551.2024	551.2028	0.69	160, 244
P2	Trihydroxylation	6.4	C23H23N2O5	407.1601	407.1599	-0.56	144, 246
P3	Dihydrodiol formation + hydroxylation	6.5	C23H25N2O5	409.1758	409.1763	1.13	144, 230
P4	Ketone formation + dihydroxylation	6.5	C23H21N2O5	405.1445	405.1449	0.97	160, 244
P5	Ketone formation + dihydroxylation	6.9	C23H21N2O5	405.1445	405.1449	1.08	144, 244
P6	PI-COOH + hydroxlyation	6.9	C14H18NO3	248.1281	248.1284	1.26	130, 144, 158, 174, 230
P7	Dihydrodiol formation + hydroxylation	7.0	C23H25N2O5	409.1758	409.1748	-2.51	144, 158 (230 is missing in QTOF but present in QqQ)
P8	Dihydrodiol formation + ketone formation	7.0	C23H23N2O5	407.1601	407.1603	0.36	144, 228
P9	Ketone formation + dihydroxylation	7.4	C23H21N2O5	405.1445	405.1448	0.62	244 (144 is missing in QTOF but present in QqQ)
P10	PI-COOH + glucosidation	7.5	C14H18NO2	394.1860	394.1858	-0.55	118, 130, 132, 144, 158, 186, 214, 232
P11	PI-COOH + hydroxlyation	7.6	C14H18NO3	248.1281	248.1283	0.92	130, 174, 230
P12	Carboxylation + hydroxylation	7.7	C23H21N2O5	405.1445	405.1443	-0.51	144, 244
P13	Dihydroxylation	7.8	C23H23N2O4	391.1652	391.1654	0.41	144, 230

P14	Dihydrodiol formation + ketone formation	7.8	C23H23N2O5	407.1601	407.1604	0.58	144, 228
P15	Dihydroxylation	8.0	C23H23N2O4	391.1652	391.1655	0.58	144, 246
P16	Dihydroxylation	8.5	C23H23N2O4	391.1652	391.1653	0.27	144, 246
P17	Ketone formation + hydroxylation	8.5	C23H21N2O4	389.1496	389.1500	1.1	144, 228
P18	Ketone formation + dihydroxylation	8.6	C23H21N2O5	405.1445	405.1444	-0.17	260 (144 is missing in QTOF but present in QqQ)
P19	Dihydroxylation	8.7	C23H23N2O4	391.1652	391.1654	0.41	144, 246
P20	Ketone formation + hydroxylation	8.9	C23H21N2O4	389.1496	389.1498	0.55	144, 228
P21	Ketone formation + hydroxylation	9.8	C23H21N2O4	389.1496	389.1498	0.56	144, 244
P22	Ketone formation + hydroxylation	10.1	C23H21N2O4	389.1496	389.1493	-0.78	144, 228
P23	Ketone formation + hydroxylation	10.8	C23H21N2O4	389.1496	389.1494	-0.35	144, 244
P24	Carboxylation	11.1	C23H21N2O4	389.1496	389.1493	-0.84	144, 244
P25	Ketone formation + hydroxylation	11.3	C23H21N2O4	389.1496	389.1500	1.1	144, 228
P26	Hydroxylation	11.5	C23H23N2O3	375.1703	375.1706	0.66	144, 230
P27	Dihydrodiol formation	12.0	C23H25N2O4	393.1809	393.1812	0.72	144, 214
P28	Hydroxylation	13.2	C23H23N2O3	375.1703	375.1695	-2.06	130, 144, 158, 230
P29	Ketone formation	13.4	C23H21N2O3	373.1547	373.1547	0.11	144, 228
P30	Ketone formation	15.1	C23H21N2O3	373.1547	373.1547	0.06	144, 228
Parent	PB-22	21.7	C23H23N2O2	359.1754	359.1757	0.85	144, 214

Supplementary Table III

XLR-11 metabolites with retention time, elemental composition, exact mass, accurate mass, mass error and diagnostic product ions.

ID	Metabolites	RT (min)	Elemental composition [M+H]	Exact mass	Accurate mass	Mass error (ppm)	Diagnostic product ions
X1	Oxidative defluorination to carboxylic acid + hydroxylation	7.5	C21H28NO4	358.2013	358.2012	-0.27	144, 244
X2	Oxidative defluorination + hydroxylation	7.7	C21H30NO3	344.2220	344.2203	-5.1	144, 230
X3	Dihydroxylation	7.8	C21H29FNO3	362.2126	362.2121	-1.49	144, 248
X4	Oxidative defluorination to carboxylic acid + hydroxylation	7.8	C21H28NO4	358.2013	358.2011	-0.38	144, 244
X5	Oxidative defluorinaton to carboxylic acid + carboxylation	7.9	C21H26NO5	372.1805	372.1807	0.35	144, 244, 354
X6	Dihydroxylation	8.0	C21H29FNO3	362.2126	362.2126	-0.13	144, 232
X7	Oxidative defluorination + hydroxylation	8.1	C21H30NO3	344.2220	344.2207	-3.79	144, 230
X8	Oxidative defluorination + carboxylation	8.1	C21H28NO4	358.2013	358.2008	-1.3	144, 230
X9	Dihydroxylation	8.1	C21H29FNO3	362.2126	362.2122	-1.22	144, 248
X10	Carboxylation + hydroxylation	8.4	C21H27FNO4	376.1919	376.1915	-1.01	130, 144, 248, 358
X11	Dihydroxylation	8.4	C21H29FNO3	362.2126	362.2123	-0.83	144, 248
X12	Dihydroxylation	8.5	C21H29FNO3	362.2126	362.2125	-0.19	144, 232
X13	Dihydroxylation	8.8	C21H29FNO3	362.2126	362.2124	-0.49	144, 232
X14	Carboxylation + glucosidation (in-source fragmentation)	8.9	C21H27FNO3	360.1969	360.1966	-0.99	144, 232, 342

X15	Oxidative defluorination to carboxylic acid + aldehyde formation	9.0	C21H26NO4	356.1856	356.1854	-0.7	144, 244
X16	Oxidative defluorination + aldehyde formation	9.4	C21H28NO3	342.2064	342.2061	-0.67	144, 230
X17	Oxidative defluorination to carboxylic acid + aldehyde formation	9.6	C21H26NO4	356.1856	356.1851	-1.55	144, 244
X18	Carboxylation + glucosidation (in-source fragmentation)	9.8	C21H27FNO3	360.1969	360.1965	-1.25	144, 232, 342
X19	Dihydroxylation	10.7	C21H29FNO3	362.2126	362.2124	-0.48	144, 232
X20	Dihydroxylation	11.0	C21H29FNO3	362.2126	362.2122	-0.98	144, 232
X21	Hydroxylation	11.6	C21H29FNO2	346.2177	346.2176	-0.28	144, 232
X22	Carboxylation	12.3	C21H27FNO3	360.1969	360.1967	-0.6	144, 232, 342
X23	Hydroxylation	12.8	C21H29FNO2	346.2177	346.2173	-1.01	144, 232
X24	Oxidative defluorination to carboxylic acid	13.3	C21H28NO3	342.2064	342.2059	-1.29	125, 144, 244
X25	Oxidative defluorination	14.2	C21H30NO2	328.2271	328.2265	-1.89	125, 144, 230
X26	Aldehyde formation	14.6	C21H27FNO2	344.2020	344.2017	-0.86	144, 232
Parent	XLR-11	20.9	C21H29FNO	330.2228	330.2223	-1.27	125, 144, 232

Supplementary Table IV

UR-144 metabolites with retention time, elemental composition, exact mass, accurate mass, mass error and diagnostic product ions.

ID	Metabolite	RT (min)	Elemental composition [M+H]	Exact mass	Accurate mass	Mass error (ppm)	Diagnostic product ions
U1	Trihydroxylation	6.2	C21H30NO4	360.2169	360.2165	-1.11	144, 230
U2	Trihydroxylation	6.5	C21H30NO4	360.2169	360.2166	-0.82	144, 230
U3	Trihydroxylation	7.3	C21H30NO4	360.2169	360.2165	-1.27	144, 230
U4	N-dealkylation + hydroxylation	7.5	C16H20NO2	258.1489	258.1487	-0.68	116, 144
U5	Trihydroxylation	7.6	C21H30NO4	360.2169	360.2163	-1.73	144, 230
U6	Carboxylation + hydroxylation	7.6	C21H28NO4	358.2013	358.2009	-1.15	144, 244
U7	Dihydroxylation	7.8	C21H30NO3	344.2220	344.2215	-1.6	144, 230
U8	Carboxylation + hydroxylation	7.9	C21H28NO4	358.2013	358.2009	-1.16	144, 244
U9	N-dealkylation + hydroxylation	7.9	C16H20NO2	258.1489	258.1490	0.43	116, 144
U10	Carboxylation + hydroxylation	8.2	C21H28NO4	358.2013	358.2007	-1.76	144, 230, 340
U11	Dihydroxylation	8.3	C21H30NO3	344.2220	344.2216	-1.25	144, 230
U12	Carboxylation + hydroxylation	8.5	C21H28NO4	358.2013	358.2014	0.28	144, 230, 340
U13	Dihydroxylation	8.6	C21H30NO3	344.2220	344.2218	-0.51	144, 230
U14	Ketone formation + hydroxylation	8.8	C21H28NO3	342.2064	342.2061	-0.78	144, 228
U15	Carboxylation + hydroxylation	9.2	C21H28NO4	358.2013	358.2007	-1.56	130, 144, 158, 230, 340

U16	Dihydroxylation	9.2	C21H30NO3	344.2220	344.2217	-0.95	144, 230
U17	Ketone formation + carboxylation	9.3	C21H26NO4	356.1856	356.1855	-0.24	144, 228, 338
U18	Ketone formation + hydroxylation	9.5	C21H28NO3	342.2064	342.2061	-0.76	144, 228
U19	Aldehyde formation + hydroxylation	9.6	C21H28NO3	342.2064	342.2059	-1.25	144, 230
U20	Ketone formation + carboxylation	10.3	C21H26NO4	356.1856	356.1854	-0.61	130, 144, 228, 338
U21	Aldehyde formation + ketone formation	11.1	C21H26NO3	340.1907	340.1910	0.82	144, 228
U22	Hydroxylation	14.4	C21H30NO2	328.2271	328.2264	-2.04	125, 144, 230
U23	Hydroxylation	14.7	C21H30NO2	328.2271	328.2268	-0.79	125, 144, 230
U24	Hydroxylation	15.3	C21H30NO2	328.2271	328.2268	-1.02	144, 214
U25	Hydroxylation	17.4	C21H30NO2	328.2271	328.2266	-1.5	144, 214
Parent	UR-144	26.1	C21H30NO	312.2322	312.2320	-0.72	125, 144, 214